Altered nanofeature size dictates stem cell differentiation

Farouk Zouani O, Christel Chanseau, Brigitte Brouillaud, Reine Barielle, Florent Deliane, Marie-Pierre Foulc, Ahmad Mehdi, Marie-Christine Durrieu

Altered nanofeature size dictates stem cell differentiation

Omar F. Zouani[1,2,*], Christel Chanseau[1,2], Brigitte Brouillaud[1,2], Reine Bareille[1,2], Florent Deliane[3], Marie-Pierre Foulc[3], Ahmad Mehdi[4] and Marie-Christine Durrieu[1,2]

[1]INSERM, U1026, BioIngénierie Tissulaire, F-33076 Bordeaux, France
[2]Université Bordeaux, 146 rue Léo Saignât, F-33076 Bordeaux, France
[3]RESCOLL Société de Recherche, F-33615 Pessac, France
[4]Institut Charles Gerhardt, UMR 5253 CNRS, Chimie Moléculaire et Organisation du Solide, Université Montpellier II, Place E Bataillon, F-34095 Montpellier, France

*Author for correspondence (omar.zouani@inserm.fr)

Accepted 14 October 2011
Journal of Cell Science 125, 1217–1224

doi: 10.1242/jcs.093229

Summary

The differentiation of stem cells can be modulated by physical factors such as the micro- and nano-topography of the extracellular matrix. One important goal in stem cell research is to understand the concept that directs differentiation into a specific cell lineage in the nanoscale environment. Here, we demonstrate that such paths exist by controlling only the micro- and nano-topography of polymer surfaces. Altering the depth (on a nanometric scale) of micro-patterned surface structures allowed increased adhesion of human mesenchymal stem cells (hMSCs) with specific differentiation into osteoblasts, in the absence of osteogenic medium. Small (10 nm) depth patterns promoted cell adhesion without noticeable differentiation, whereas larger depth patterns (100 nm) elicited a collective cell organization, which induced selective differentiation into osteoblast-like cells. This latter response was dictated by stress through focal-adhesion-induced reorganization of F-actin filaments. The results have significant implications for understanding the architectural effects of the in vivo microenvironment and also for the therapeutic use of stem cells.

Key words: Cell differentiation, Mesenchymal stem cells, Osteogenesis, Nanotopography, Surface functionalization

Introduction

A crucial element of tissue engineering is to create a favorable extracellular microenvironment, mainly of the extracellular matrix (ECM), to guide cell differentiation and tissue regeneration. Indeed, it has been observed that macro-, micro- and nano-sized topographical factors stimulate behavioral changes in both cells and tissues (Curtis and Varde, 1964; Webster et al., 2000; Nayak et al., 2010). Recent studies related to the importance of nanometric scale surface topography (variation in x and y distances) and roughness of biomaterials, rather than chemical modification of the surface, have significantly highlighted a direct correlation between this nano-topography and cell survival (Park et al., 2007; Oh et al., 2009; Dalby et al., 2007b; Dalby et al., 2006). It is clear that interplay exists between cells and nanoscale features. In vivo, cells will encounter many topographical features ranging from folded proteins to the ECM. The physical and mechanical cues of ECM are transduced into intracellular rheological and biochemical changes through unknown mechanisms, but probably through conformational changes or unfolding of focal-adhesion-based proteins (Del Rio et al., 2009; Grashoff et al., 2010) and other proteins. Several researchers have also proposed that intracellular rheological properties are crucial for understanding cell behavior (Chowdhury et al., 2010; Weitz et al., 2008; Mizuno et al., 2007; Trepat et al., 2007). Therefore to facilitate this research, in vitro studies represent an interesting study model.

Here, we demonstrate such paths by controlling the nano-topography of polyethylene terephthalate (PET) surfaces. Altering the dimensions of the nano-depths of micro-patterned surface structures allowed an increase in human mesenchymal stem cell (hMSC) adhesion, with specific differentiation into osteoblasts. We demonstrate that larger depth patterns (100 nm) elicited a collective cell organization, which induced selective differentiation towards an osteoblastic phenotype. This latter response was dictated by stress through focal adhesions, which induced reorganization of F-actin filaments. Small (10 nm) depth patterns promoted cell adhesion without noticeable differentiation. Nanocues, such as those presented here, might prove to be important in tissue-specific stem cell differentiation. The results have significant implications for understanding the architectural effects of the in vivo microenvironment. For effective tissue engineering using hMSCs, it is important to develop optimized cell culture differentiation conditions based upon the influence of the microenvironment.

Results

Here we report on the response of cells seeded onto materials showing defined depth variation (disordered micropatterns with different depth heights of 10–100 nm). To do this, we developed a protocol of surface treatment using PET, which enabled control of the micro- and nano-topography. This is based on previous work showing that PET is photo-degraded under the effect of ultraviolet (UV) radiation (Fechine et al., 2004; Wang et al., 1999). Here, we exposed the PET for various durations to UV. Depending on the duration of irradiation with UV (15 to

Journal of Cell Science

60 hours), we obtained micropatterns with various depths (Fig. 1A,B). Detailed experimental descriptions can be found in the Materials and Methods. The nano-topography was characterized using an Optical 3D Profiler System (OPS), which showed a highly disordered nano-depth, with different sizes between 10 nm and 100 nm (Fig. 1B, Fig. 2A and supplementary material Fig. S1A). All these surfaces with different characterized topographies were functionalized with peptides supporting cell adhesion (Chollet et al., 2009; Zouani et al., 2010) (supplementary material Fig. S1B,D). No differences in mechanical properties were observed in the materials used. Indeed, the elastic modulus E was measured at about 1.6 ($\pm$0.2) GPa (supplementary material Fig. S1C).

To study the unique influence of surface topography on cells, all cell adhesion experiments were carried out without any serum for the first 12 hours of culture. Adhesion peptide density (RGD peptides) was quantified here through high-resolution beta imagery using a radiolabeled amino acid ([^{3}H]lysine) (Chollet et al., 2009; Porté-Durrieu et al., 2004). Irrespective of how long the UV treatment was performed on PET (between 15 hours and 60 hours), the RGD peptide density was 2.2$\pm$0.5 pmol/mm^2 (supplementary material Fig. S1B) (Chollet et al., 2009; Porté-Durrieu et al., 2004). The RGD spacing on all surfaces was $<$1 nm.

PET functionalized with RGD peptides after UV treatment for 15 hours with a smooth surface (Fig. 1A,B) acted as a reference surface. OPS and SEM images were recorded of hMSCs cultured (without serum) on RGD-functionalized PET (using various durations of UV treatment). After incubation for 2 hours, the shapes of hMSCs sitting on the top of PET-grafted RGD and on the various nano-depths was very different (Fig. 2A,B). Indeed, using the OPS technique, we observed that projected areas of hMSCs were maximal in the case of larger depths (100 nm); the average cell thickness was also minimal at this depth compared with other conditions (Fig. 1A). hMSCs on raw PET were not adhered (results not shown). As shown in Fig. 2B (white arrows), we clearly saw small filopodia extensions of cells grown on PET-RGD after exposure to UV for 15 hours ($<$10 nm depth); whereas for larger microstructure depths, these filopodia extensions were not observed. Obviously, the larger the depth of the microstructure (100 nm), the more stable the hMSC adhesion and the better the cells spread (Fig. 2A–C). On large nano-depth surfaces, cells were totally spread, even after 2 hours of culture. Surprisingly, after 16 hours of culture, we observed that cells on large nano-depth surfaces (100 nm) adopt a special collective organization in comparison with all other surfaces (Fig. 2D). hMSCs organized in a layered network and this phenomenon was not observed on other surfaces (Fig. 2D). After prolonged incubation, these differences were eventually less apparent because of cell confluence (Fig. 3B).

Human MSC behavior (cell adhesion and collective organization) on large nano-depth surfaces resulted in a preferential differentiation into an osteogenic lineage, which was confirmed by immunoblotting and immunofluorescence staining of three common protein osteogenic markers: Runx2 (an essential transcription factor in osteoblast differentiation), Osterix (Osx, a transcriptional factor induced by Runx2, which is required for the differentiation of osteoprogenitor cells into functional osteoblasts) (Wang et al., 2011; Zhang et al., 2008), and osteopontin (OPN). This analysis for the detection of osteogenic protein expression of hMSCs was conducted on cells cultured for 1 week for Runx2 and Osx, and 3 weeks for OPN. The immunoblotting and immunofluorescence results, which are shown in Fig. 3 and supplementary material Fig. S2 for different surfaces, show that hMSCs were positive for Runx2, Osx and OPN staining in the case of large nano-depth surfaces (100 nm). In Fig. 3A and supplementary material Fig. S2, the blot and immunostaining suggest osteogenic commitment with Runx2 and Osx expression, respectively. In Fig. 3B, cells were stained with actin and OPN, and they confirm osteogenic differentiation with OPN expression.

To further support the immunofluorescence staining results, osteoblast gene expression [alkaline phosphatase (ALP), osteocalcin (OCN) and OPN] was also studied by quantitative real-time PCR analysis after 12 days of incubation (Fig. 4). Human MSCs on 100-nm-deep PET-RGD demonstrated various levels of upregulation of osteogenic genes, and showed a significantly higher level of gene expression than cells on other substrata. The 100 nm depth led to the greatest upregulation of all selected osteoblastic genes among the experimental groups after 12 days of incubation. Together, immunofluorescence and real-time PCR results confirmed that 100 nm depths have the potential to act as a guided differentiation tool for directing hMSCs into osteoblast-like cells in the absence of osteogenesis-

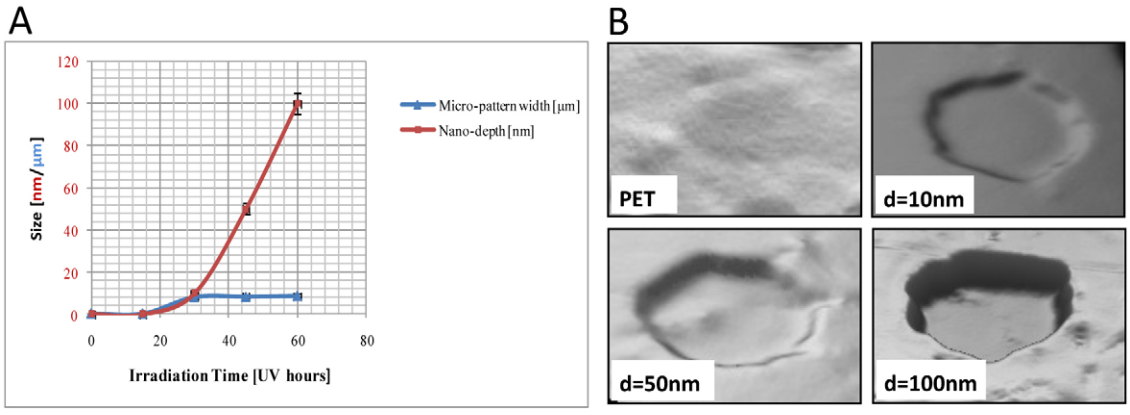

Fig. 1. Surface of PET topographies with nanoscale depths. (**A**) PET microtopography and nanoscale depths were generated by UV irradiation, the micrometric width of all patterns is about 8.5 µm ($\pm$0.5). (**B**) OPS images showing three different nanodepths: d=10, 50 and 100 nm.

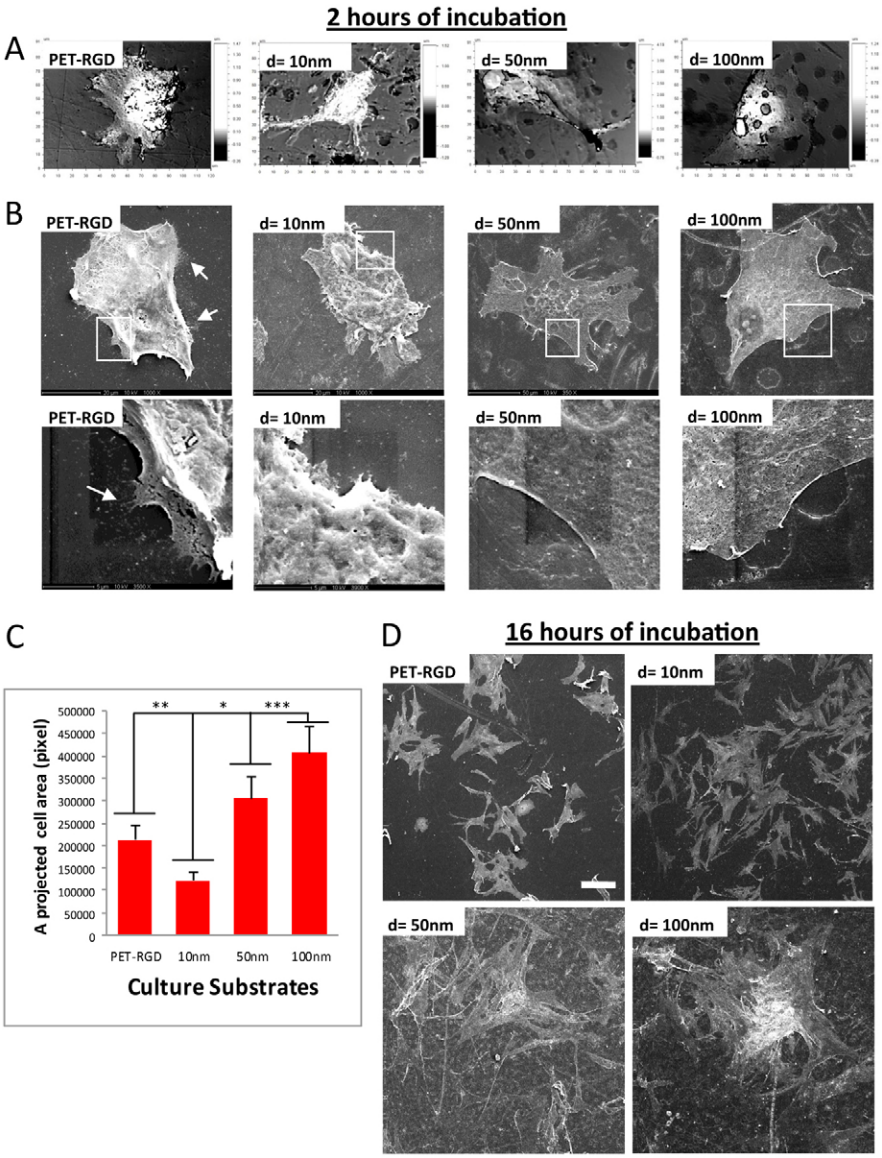

Fig. 2. Human mesenchymal stem cell adhesion. OPS (**A**) and SEM (**B**) micrographs of hMSCs on smooth PET (control) and 10, 50, 100 nm depth PET-RGD surfaces after 2 hours of culture. Cells are flat, spread out or round depending on the substrate; they become progressively more spread out as the nano-depth is increased to 100 nm. (**C**) Influence of surface topography on hMSC spreading 2 hours after seeding (*P<0.05; **P<0.01; ***P<0.001). (**D**) A high level of cell organization is induced on nano-depths of 100 nm, especially after 16 hours of culture. Scale bar: 50 μm.

inducing medium. By contrast, the cells grown on 10-nm-deep PET-RGD exhibited a significantly lower degree of osteoblast gene expression (Fig. 4).

Discussion

The aim of this work was to study adhesion and differentiation of hMSCs seeded onto RGD-functionalized PET surfaces offering controlled topographies (pattern sizes varying between 10 and 100 nm); all experiments were performed in the absence of serum because it contains proteins that are likely to adsorb onto materials and thus influence cell behavior. As a result, in the presence of serum, a new parameter comes into consideration: the amount and quality of adsorbed proteins onto surfaces. Park and Oh and colleagues (Park et al., 2007; Oh et al., 2009) have shown that stem cells are oriented towards an osteoblastic lineage by altering the dimension of titanium nanotubes. Even though both these authors used the same ‘model’ material, i.e. titanium nanotubes with diameters of 10–100 nm, no consensus was found as far as stem cell behavior on these materials is concerned. Indeed, Park and co-workers (Park et al., 2007) demonstrate that a spacing of 15 nm and not 100 nm provided an effective scale to differentiate hMSCs into osteoblast-like cells; however, Oh et al. (Oh et al., 2009) showed completely the opposite. The contradictory results reported by these authors might be due to several factors: we believe that one influential factor on cell adhesion in the first hours of culture is the adsorption of proteins on the surface (Dolatshahi-Pirouz et al., 2010). Oh and colleagues (Oh et al., 2009) detected fibronectin as well as albumin on surfaces (TiO_2 nanotubes). They observed nanometer-sized aggregates on the nano-topography surfaces. In our study, to avoid any possible influence of different proteins adsorbed onto the surface material [because qualitative and quantitative adsorption of biomolecules is correlated to surface physico-chemical parameters (Dolatshahi-Pirouz et al., 2010)], we focused on functionalizing the polymer surface using adhesion peptides (RGD peptides) of consistent density. Consequently, only surface micro- and nano-topography varies with this material. Stem cells are very sensitive to both the physical and

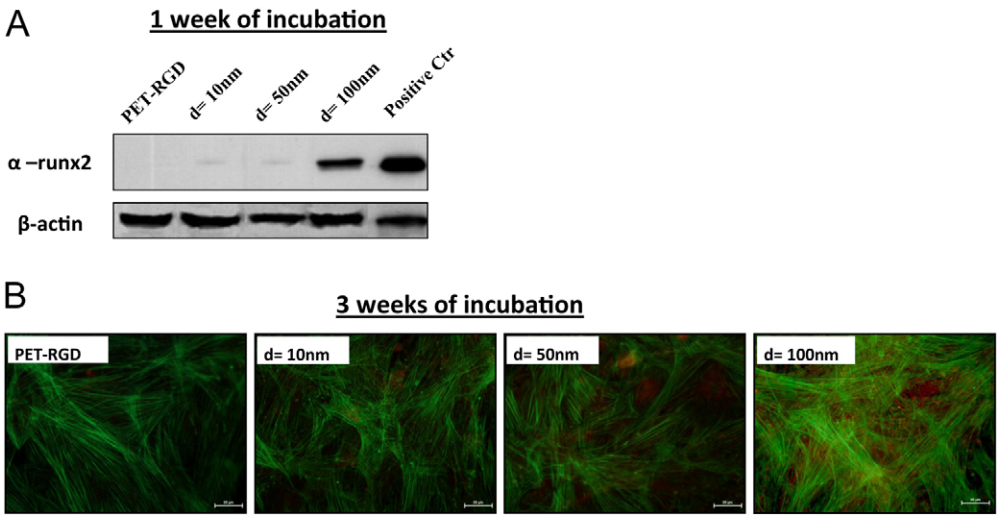

Fig. 3. Human mesenchymal stem cell differentiation. Stem cells after 1 week (**A**) and 3 weeks (**B**) in culture differentiate into osteoblast-like cells on surfaces with 100 nm depth as seen by Runx2 blotting and OPN staining, respectively. Actin, green; OPN, red. Scale bars: 50 μm.

biochemical microenvironment (McBeath et al., 2004). The results presented in Fig. 2 clearly show that hMSCs adhered to the smooth and biggest depths more efficiently (spreading) in the first 2 hours, probably because of the high RGD population initially grafted covalently on the surface. However, in comparison, as indicated in SEM micrographs, the greatest depth (100 nm) that induced collective cell organization also led to the increased expression of osteogenic genes (Figs 3,4) and displayed a larger number of adhered cells.

Furthermore, our experimental results indicated that the hMSCs were significantly more organized in multilayer networks and were probably stressed on the 100-nm-depth surface. It is probable that this type of cell adhesion and collective organization causes cellular cytoskeletal tension and stress on the hMSCs compared with normal cell culture conditions on a flat surface substrate (Fig. 5a,c,e–h). Stem cell differentiation in a specific lineage with stress was studied in the presence of materials with various elasticities (Chowdhury et al., 2010; McBeath et al., 2004; Yamamoto et al., 2005; Saretzki et al., 2008; Altman et al., 2002; Norgaard et al., 2006). It also

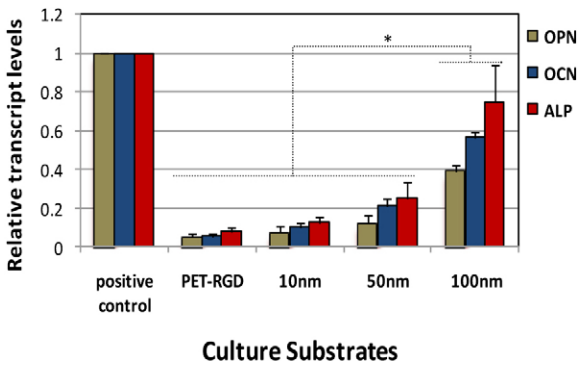

Fig. 4. Quantitative PCR analysis of alkaline phosphatase, osteoclacin and osteopontin. Plastic cell culture plate with osteogenesis-inducing medium was used as a positive control for osteogenic differentiation. Significant differences were observed between 100 nm depths vs other groups, for OPN, OCN and ALP gene expression (*$P<0.01$).

seems that this type of cell adhesion (contact focal maturation, reorganization of actin filaments) and then cell organization is due to the maturation of focal contacts on the hMSCs cultured on 100-nm-deep substrate. Indeed, integrin clustering and maturation are important for hMSC adhesion and differentiation onto osteoblast-like cells (Park et al., 2007; Hamidouche et al., 2009). The present results indicate that a depth of 100 nm provides the nano-structure scale for actin network organization and integrin clustering (Fig. 5b,e,g,h and Fig. 6A), and differentiation at a higher rate than on smooth PET-RGD and 10-nm-deep PET-RGD. To confirm these conclusions, hMSCs were incubated for 1 hour after 6 hours of cell seeding with cytochalasin D (actin polymerization inhibition) or jasplakinolide (actin stabilization). In these two cases, the differentiation of hMSCs onto osteoblast-like cells was inhibited (supplementary material Fig. S3A–C). Indeed, the disruption of the actin networks induced by treatment with cytochalasin D resulted in minimal actin tension and ultimately led to a more rounded morphology, suggesting that cell shape has a significant role in hMSC differentiation. However, inhibition of cell reorganization with jasplakinolide blocks hMSC differentiation (supplementary material Fig. S3A–C). These results indicate that an intact actin network is responsible for hMSC differentiation in our in vitro system.

From the results of our research comes a concept of stem cell fate based on the microtopography and nano-depth dimensions, which is illustrated in Fig. 6B. This suggested mechanism is, in a sense, in agreement with the general notion that when hMSCs are busy adhering and growing, their functionality is reduced, but when the stem cells are stressed (Dalby et al., 2007b; Chowdhury et al., 2010) and have mature focal contacts (Park et al., 2007), they tend to differentiate into an osteoblast lineage.

The collective organization observed here generates special interactions and orientations of hMSCs, thus resulting in the generation of an intracellular force (Tambe et al., 2011). This ends with mechanical signal transduction between cells. In addition, by observing the organization of hMSCs on 100-nm-deep surfaces, there is a collective circular organization (Tambe et al., 2011; Stockholm et al., 2010). Most likely, this cell organization is probably generated by the specific organization of actin filaments and focal contacts on 100-nm-deep surfaces

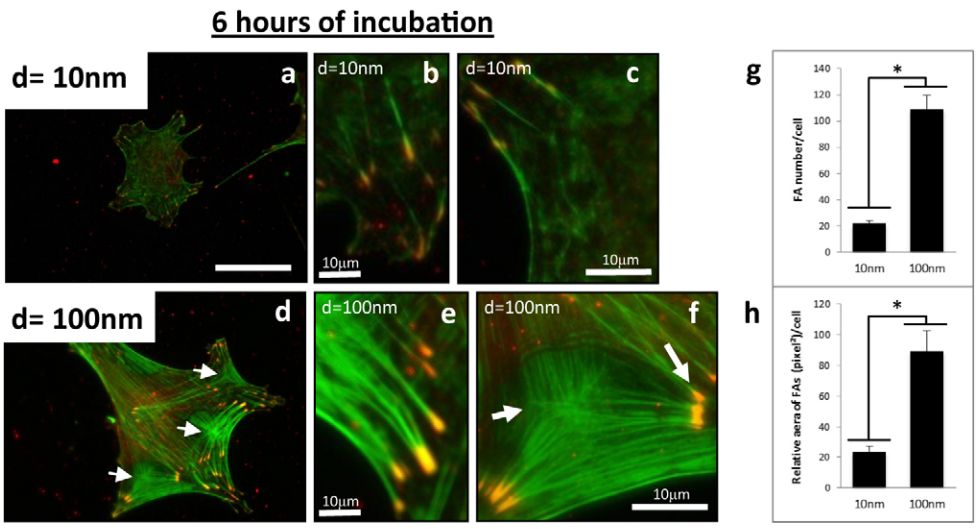

Fig. 5. Focal contact formation and actin network organization. (**a**–**f**) After 6 hours of seeding at 10 and 100 nm depths, focal contact formation and special stress fiber assembly (arrows in d and f) was extensive on 100 nm depths (d,e) as shown by staining for vinculin (red) and phalloidin (green), but strongly reduced on 10 nm depths (a,b). Scale bars: 50 µm (a,d); 10 µm (b,c,e,f). (**g**,**h**) hMSC number of focal contacts (g) and relative area of contacts (h) on 10-nm- and 100-nm-deep surfaces (*P<0.05).

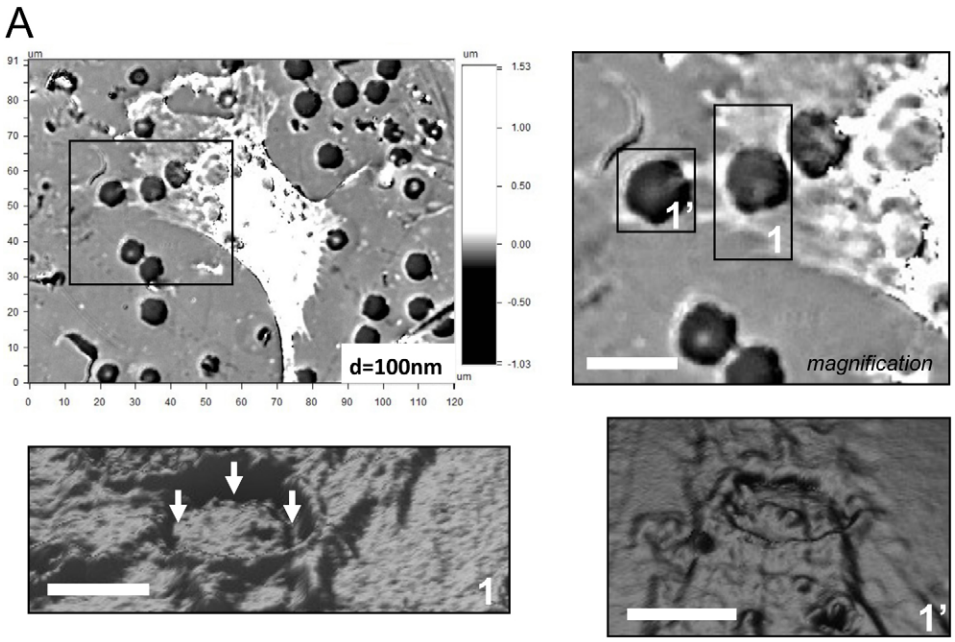

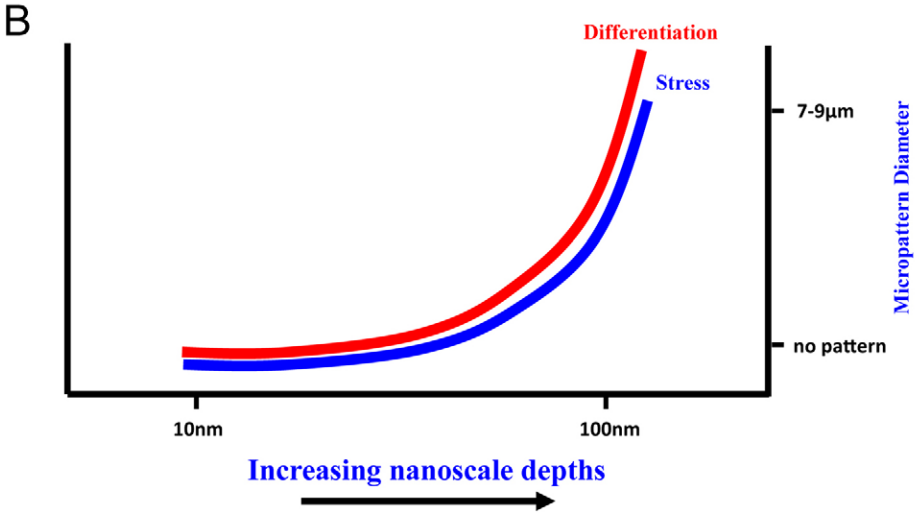

Fig. 6. Mechanism of hMSC osteogenic differentiation induced by selective nanosizing. (**A**) OPS micrographs of hMSCs cultured for 2 hours on surfaces with 100 nm depths. 1 and 1′ show OPS micrograph 3D reconstruction. Cell deformation is induced (arrows). Scale bars: 10 µm. (**B**) Schematic illustration of the overall trends of nanocue effects on hMSC fate and morphology in the first 16 hours of culture. The change in stressed hMSCs (adhesion and cytoskeleton organization) evolves in the same way (progression) as differentiation. In our model, evolution of adhesion (focal adhesion area and number, Fig. 5) correlates with the activation of protein complexes by stress, generating the folding–unfolding balance.

(Fig. 2D, Figs 5, 6 and supplementary material Fig. S3), resulting in a maximal stress, as demonstrated by Tambe and colleagues (Tambe et al., 2011). This process might explain the commitment of hMSCs towards the osteoblastic lineage.

Nanocues, such as those presented here, might prove to be important in tissue-specific stem cell differentiation. These findings are supported by recent observations that chemical stimulation (Huang et al., 2005a; Huang et al., 2005b), chemical patterning (McBeath et al., 2004) and material stiffness (Engler et al., 2006) all have roles in stem cell differentiation. These studies indicate the importance of any discrete change in the stem cell environment and the need to elucidate the function of the stem cell niche. One of the initial events that allows induction of stem cell differentiation through a material is the formation of mature focal contacts, (Fig. 5, Fig. 6A and supplementary material Fig. S3). These changes in adhesion formation will impact cytoskeletal tension, because adhesion forms the anchoring points for the cytoskeleton. Such changes in cytoskeletal tension will have an effect on indirect mechanotransductive pathways, as demonstrated by changes in levels of RhoA in stem cells in response to material stiffness (McBeath et al., 2004; Engler et al., 2006) or external stress (Chowdhury et al., 2010) and here, in the case of materials presenting nanotopographies with a depth of 100 nm (Fig. 5, Fig. 6A and supplementary material Fig. S3). It has also been speculated that changes in cytoskeletal tension in response to topography, could change interphase nucleus organization and hence more directly influence the cellular gene expression profile (Dalby et al., 2007a). These changes in adhesion and cytoskeleton will impose morphological changes on cells, as noted for cells cultured on materials presenting depths of 100 nm. In our case, we found the specific organization of the focal-adhesion–cytoskeleton complex showing a probable alteration of focal-adhesion-based proteins. This can result from the activation and maturation of focal adhesions. For example, in vitro experiments show that the unfolding of single talin rods activates vinculin binding (Del Rio et al., 2009; Grashoff et al., 2010). This latter process seems to form part of the molecular mechanism of mechanotransduction in the cell.

The identification of mechanisms that direct adult hMSC osteogenic differentiation is of prime interest for developing therapeutic strategies to promote bone formation and repair. In this study, we establish the essential role of nanoscale in hMSC differentiation and show that specific stress through the focal-adhesion–cytoskeleton complex is sufficient to promote osteoblast differentiation. This provides a tool to promote hMSC osteogenic capacity, which could be exploited for bone tissue engineering and repair.

Materials and Methods

PET surface preparation and covalent grafting of RGD peptide

PET surfaces (commercial bi-oriented film with a thickness of 100 μm obtained from Goodfellow, France) were used for producing microtopography and nanotopography surfaces. PET was exposed to UV (254 nm) for various periods ranging from 15 to 60 hours on each side. This irradiation step creates acid carboxyl end groups and mono or dihydroxy terephthalate (Fechine et al., 2004). This weakens the PET and makes it sensitive to any physical and/or chemical treatment thereafter (Fechine et al., 2004; Wang et al., 1999). We sonicated the surface for 15 minutes. Polymer surfaces were modified according to a published method (Chollet et al., 2009). Briefly, materials were modified in order to create COOH functions on PET surfaces [with 5 g $KMnO_4$ and 100 ml H_2SO_4 (1.2N) at 60℃]. Next, PET-COOH samples were immersed in a solution of 0.2 M EDC (dimethylaminopropyl-3-ethylcarbodiimide hydrochloride) and 0.1 M NHS (N-hydroxysuccinimide) in 0.1 M MES buffer [2-(N-morpholino)-ethanesulfonic acid] in MilliQ water and then rinsed in 50 ml MilliQ water for 30 minutes. The same protocol was used for each surface. Finally, immobilization of RGD (Arg-Gly-Asp) (or [^{3}H]lysine instead of RGD peptides in the case of high resolution beta-imager) (Chollet et al., 2009) peptides was achieved in a solution of peptides in 1× PBS ($C=10^{-3}$ M) for 15 hours at room temperature. After grafting, the disks were rinsed with 100 ml MilliQ water for 1 week. Surfaces were characterized using X-ray photoelectron spectroscopy (XPS) and a high-resolution beta-imager (Chollet et al., 2009). Our results showed that the density of RGD grafted onto PET remains the same, whatever the duration of UV irradiation. The spacing of RGD immobilized on the surface of PET was calculated according to a published method (Massia and Hubbell, 1991).

Characterization of mechanical properties

The elastic moduli (E) of the topcoats were determined by the nanoindentation technique (NHT, CSM Instruments) following the Oliver and Pharr method (Oliver and Pharr, 1992). Nanoindentation is an indentation technique that allows the determination of the elastic modulus of materials by measuring the force applied on the PET (RGD-functionalized PET using various UV treatment times) versus the indentation depth.

Cell culture

Primary human MSCs were obtained according to methods described previously (Li et al., 2010). Briefly, we aspirated bone marrow from the femoral diaphysis or iliac bone after obtaining consent from patients (aged 20–70 years) undergoing hip prosthesis surgery after trauma. The human bone marrow was sequentially filtered with syringes fitted with 16-, 18- and 21-gauge needles, and cells were cultured in Minimum Essential Medium (Alpha-MEM, GIBCO) supplemented with 10% (v/v) FBS and 1% penicillin-streptomycin, and incubated in a humidified atmosphere containing 5% (v/v) CO_2 at 37℃. All cell culture experiments were carried out without serum for the first 12 hours of culture. The permission to use bone marrow was granted by the Pellegrin Hospital committee and AD INSERM for research involving human subjects of the University of Bordeaux 2; this consent was obtained under the supervision of Joëlle Amédée (INSERM U1026, France). All cells were used at low passage numbers (passage 2), were subconfluently cultured, and were seeded at 10^4 cells/cm^2 for experiments. In this study, we conducted all experiments in parallel with hMSCs from Lonza (Switzerland; Cat. no. PT-2501). For a positive control, we used osteogenesis-inducing medium containing dexamethasone (10^{-8} M), acid ascorbic (50 mg/ml) and β-glycerophosphate (8 mM). The following pharmacological agents were used: 1 μM cytochalasin D (Sigma) and 50 nM jasplakinolide (Invitrogen). hMSCs were exposed to each pharmacological agent for 1 hour after seeding every 24 hours for 3 days.

Optical 3D profiling system (OPS)

Wyko surface profiler systems (Veeco-NT1100) are non-contact optical profilers that use two technologies to measure a wide range of surface heights. The phase-shifting interferometry (PSI) mode allows measuring smooth surfaces and small steps, whereas the vertical scanning interferometry (VSI) mode allows measurement of rough surfaces and steps up to several micrometers high. The PSI mode was used to determine the nano-topography of surfaces. We used the VSI mode to measure the thickness of cells on the substrata. To achieve this, we fixed cells with 4% paraformaldehyde in PBS for 30 minutes at 4℃ and then we dehydrated the cells with ethanol and metallized samples with gold. Wyko Vision V3.60 software was used for 3D reconstruction of OPS images.

Scanning electron microscopy (SEM)

Initially cells were seeded on the substrates at a density of 1×10^4 cells/ml. After 2 hours and 16 hours of culture, cells were washed with 1× PBS and fixed with paraformaldehyde in PBS (4%) for 20 minutes at 4℃. Samples were dehydrated in increasing concentrations of ethanol (30, 70, 80, 90, 95 and 100%) and critical point dried. Replicas were gold-coated and observed with a scanning electron microscope (Hitachi S2500) at 10 kV.

Immunostaining

After 6 hours or 3 weeks of culture, the cells on the surfaces were fixed for 30 minutes in 4% paraformaldehyde in PBS at 4℃. After fixation, the cells were permeabilized in 1% Triton X-100 in PBS for 15 minutes. After 6 hours, cell cytoskeletal F-actin was visualized by treating the cells with 5 U/ml Alexa Fluor 488 phalloidin (Sigma) for 1 hour at 37℃. Vinculin was visualized by treating the cells with 1% (v/v) monoclonal anti-vinculin (clone hVIN-1 antibody produced in mouse) for 1 hour at 37℃. Then Alexa Fluor 568 rabbit anti-mouse IgG was added for 30 minutes at room temperature. After 1 week, Osterix was visualized by treating the cells with 1% (v/v) monoclonal anti-osterix antibody (produced in rabbit) for 1 hour at 37℃ and Alexa Fluor 568 mouse anti-rabbit IgG for 30 minutes at room temperature. After 3 weeks, actin and OPN were visualized by treating the cells with 1% (v/v) Alexa Fluor 488 Phalloidin and monoclonal anti-OPN (Abcam, Cambridge, UK), for 1 hour at 37℃ and Alexa Fluor 588 goat anti-rabbit IgG for 30 minutes at room temperature. Neuronal cytoskeletal marker β3-

tubulin [anti-β3-tubulin (Sigma)] and muscle transcription factor MyoD1 [anti-MyoD1 (Santa Cruz Biotechnology)] were not detected on hMSCs cultured on different surfaces for 1 week (results not shown).

For quantification of the size and area of focal adhesions (vinculin), we used the freeware image analysis software ImageJ. We opened the raw image, converted it to an 8-bit file, and used the unsharp mask feature (settings 1:0.2) before removing the image background (rolling ball radius 10). After smoothing, the resulting image, which appears similar to the original photomicrograph but with minimal background, was then converted to a binary image by setting a threshold. Threshold values were determined empirically by selecting a setting, which gave the most accurate binary image for a subset of randomly selected photomicrographs with varying peptide densities. The cell area was determined by manual delineation on raw fluorescent images, total contact area and mean contact area per cell were calculated by 'analyse particles' in ImageJ, contacts smaller than 3 pixels were not taken into account. A minimum of 20 cells per condition were analyzed (Chollet et al., 2009).

Real-time PCR analysis

mRNA was analyzed by quantitative RT-PCR as described previously (Zouani et al., 2010). Briefly, after 2 weeks of culture, total RNA was extracted using the RNeasy total RNA kit from Qiagen according to the manufacturer's instructions. Purified total RNA was used to make cDNA by reverse transcription (Gibco) with random primers (Invitrogen). Real-time PCR was performed with SYBR green reagents (Bio-Rad). Expression of target genes was normalized according to the GAPDH gene reference by the ΔCt method. Data were analyzed with iCycler IQ software. Results were obtained from two series of experiments performed in triplicate. In the study of hMSC differentiation, all levels of expression were normalized to the level of expression of positive control (MSCs cultured with osteogenesis-inducing medium). Primers used for amplification are listed in supplementary material Table S1.

Western blotting

After 1 week, cells were permeabilized (10% SDS, 25 mM NaCl, 10 nM pepstatin and 10 nM leupeptin in distilled water and loading buffer), boiled for 10 minutes and resolved by reducing PAGE (Invitrogen). Proteins were transferred onto nitrocellulose, blocked, and labeled with HRP-conjugated antibodies (Invitrogen). Runx2 was blotted by treating the nitrocellulose with monoclonal anti-Runx2 (Abcam, Cambridge). Our western blot was run in triplicate, along with an additional blot for actin and Coomassie Blue staining to ensure consistent protein load between samples.

Statistical analysis

All data are expressed as mean ± s.e., and analyzed statically by the paired Student's *t*-test method. Significant difference was determined at $P<0.01$.

Acknowledgements

Thanks to C. Bourget for help with western blotting.

Funding

The authors thank the Région Aquitaine, the GIS Advanced Materials in Aquitaine as well as the Agence Nationale pour la Recherche (ANR) for financial support.

Supplementary material available online at
http://jcs.biologists.org/lookup/suppl/doi:10.1242/jcs.093229/-/DC1

References

Altman, G. H., Horan, R. L., Martin, I., Farhadi, J., Stark, P. R., Volloch, V., Richmond, J. C., Vunjak-Novakovic, G. and Kaplan, D. L. (2002). Cell differentiation by mechanical stress. *FASEB J.* **16**, 270-272.

Chollet, C., Chanseau, C., Remy, M., Guignandon, A., Bareille, R., Labrugère, C., Bordenave, L. and Durrieu, M. C. (2009). The effect of RGD density on osteoblast and endothelial cell behavior on RGD-grafted polyethylene terephthalate surfaces. *Biomaterials* **30**, 711-720.

Chowdhury, F., Na, S., Li, D., Poh, Y. C., Tanaka, T. S., Wang, F. and Wang, N. (2010). Material properties of the cell dictate stress-induced spreading and differentiation in embryonic stem cells. *Nat. Mater.* **9**, 82-88.

Curtis, A. S. and Varde, M. (1964). Control of cell behavior: topological factors. *J. Natl Cancer Inst.* **33**, 15-26.

Dalby, M. J., McCloy, D., Robertson, M., Agheli, H., Sutherland, D., Affrossman, S. and Oreffo, R. O. (2006). Osteoprogenitor response to semi-ordered and random nanotopographies. *Biomaterials* **27**, 2980-2987.

Dalby, M. J., Biggs, M. J., Gadegaard, N., Kalna, G., Wilkinson, C. D. and Curtis, A. S. (2007a). Nanotopographical stimulation of mechanotransduction and changes in interphase centromere positioning. *J. Cell Biochem.* **100**, 326-338.

Dalby, M. J., Gadegaard, N., Tare, R., Andar, A., Riehle, M. O., Herzyk, P., Wilkinson, C. D. and Oreffo, R. O. (2007b). The control of human mesenchymal cell differentiation using nanoscale symmetry and disorder. *Nat. Mater.* **6**, 997-1003.

Del Rio, A., Perez-Jimenez, R., Liu, R., Roca-Cusachs, P., Fernandez, J. M. and Sheetz, M. P. (2009). Stretching single talin rod molecules activates vinculin binding. *Science* **323**, 638-641.

Dolatshahi-Pirouz, A., Jensen, T., Kraft, D. C., Foss, M., Kingshott, P., Hansen, J. L., Larsen, A. N., Chevallier, J. and Besenbacher, F. (2010). Fibronectin adsorption, cell adhesion, and proliferation on nanostructured tantalum surfaces. *ACS Nano.* **4**, 2874-2882.

Engler, A. J., Sen, S., Sweeney, H. L. and Discher, D. E. (2006). Matrix elasticity directs stem cell lineage specification. *Cell* **126**, 677-689.

Fechine, G. J. M., Rabellob, M. S., Souto Maiora, R. M. and Catalani, L. H. (2004). Surface characterization of photodegraded poly(ethylene terephthalate). The effect of ultraviolet absorbers. *Polymer* **45**, 2303-2308.

Grashoff, C., Hoffman, B. D., Brenner, M. D., Zhou, R., Parsons, M., Yang, M. T., McLean, M. A., Sligar, S. G., Chen, C. S., Ha, T. et al. (2010). Measuring mechanical tension across vinculin reveals regulation of focal adhesion dynamics. *Nature* **466**, 263-266.

Hamidouche, Z., Fromigué, O., Ringe, J., Häupl, T., Vaudin, P., Pagès, J. C., Srouji, S., Livne, E. and Marie, P. J. (2009) Priming integrin alpha5 promotes human mesenchymal stromal cell osteoblast differentiation and osteogenesis. *Proc. Natl. Acad. Sci. USA* **106**, 18587-18591.

Huang, Y. C., Kaigler, D., Rice, K. G., Krebsbach, P. H. and Mooney, D. J. (2005a). Combined angiogenic and osteogenic factor delivery enhances bone marrow stromal cell-driven bone regeneration. *J. Bone Miner. Res.* **20**, 848-857.

Huang, Y. C., Simmons, C., Kaigler, D., Rice, K. G., Mooney, D. J. (2005b). Bone regeneration in a rat cranial defect with delivery of PEI-condensed plasmid DNA encoding for bone morphogenetic protein-4 (BMP-4). *Gene Ther.* **12**, 418-426.

Li, H., Daculsi, R., Grellier, M., Bareille, R., Bourget, C. and Amedee, J. (2010). Role of neural-cadherin in early osteoblastic differentiation of human bone marrow stromal cells cocultured with human umbilical vein endothelial cells. *Am. J. Physiol. Cell Physiol.* **299**, C422-C430.

Massia, S. P. and Hubbell, J. A. (1991). An RGD spacing of 440 nm is sufficient for integrin alpha V beta 3-mediated fibroblast spreading and 140 nm for focal contact and stress fiber formation. *J. Cell Biol.* **114**, 1089-1100.

McBeath, R., Pirone, D. M., Nelson, C. M., Bhadriraju, K. and Chen, C. S. (2004). Cell shape, cytoskeletal tension, and RhoA regulate stem cell lineage commitment. *Dev. Cell* **6**, 483-495.

Mizuno, D., Tardin, C., Schmidt, C. F. and Mackintosh, F. C. (2007). Nonequilibrium mechanics of active cytoskeletal networks. *Science* **315**, 370-373.

Nayak, T. R., Jian, L., Phua, L. C., Ho, H. K., Ren, Y. and Pastorin, G. (2010). Thin films of functionalized multiwalled carbon nanotubes as suitable scaffold materials for stem cells proliferation and bone formation. *ACS Nano.* **4**, 7717-7725.

Norgaard, R., Kassem, M. and Rattan, S. I. (2006). Heat shock-induced enhancement of osteoblastic differentiation of hTERT-immortalized mesenchymal stem cells. *Ann. NY Acad. Sci.* **1067**, 443-447.

Oh, S., Brammer, K. S., Li, Y. S., Teng, D., Engler, A. J., Chien, S. and Jin, S. (2009). Stem cell fate dictated solely by altered nanotube dimension. *Proc. Natl. Acad. Sci. USA* **106**, 2130-2135.

Oliver, W. C. and Pharr, G. M. (1992). An Improved Technique for Determining Hardness and Elastic Moduli using Load and Displacement Sensing Indentation Experiments. *J. Mat. Res.* **7**, 1564-1583.

Park, J., Bauer, S., von der Mark, K. and Schmuki, P. (2007). Nanosize and vitality: TiO2 nanotube diameter directs cell fate. *Nano Lett.* **7**, 1686-1691.

Porté-Durrieu, M. C., Guillemot, F., Pallu, S., Labrugère, C., Brouillaud, B., Bareille, R., Amédée, J., Barthe, N., Dard, M. and Baquey, C. h. (2004). Cyclo-(DfKRG) peptide grafting onto Ti-6Al-4V: physical characterization and interest towards human osteoprogenitor cells adhesion. *Biomaterials* **25**, 4837-4846.

Saretzki, G., Walter, T., Atkinson, S., Passos, J. F., Bareth, B., Keith, W. N., Stewart, R., Hoare, S., Stojkovic, M., Armstrong, L. et al. (2008). Downregulation of multiple stress defense mechanisms during differentiation of human embryonic stem cells. *Stem Cells* **26**, 455-464.

Stockholm, D., Edom-Vovard, F., Coutant, S., Sanatine, P., Yamagata, Y., Corre, G., Le Guillou, L., Neildez-Nguyen, T. M. and Pàldi, A. (2010) Bistable cell fate specification as a result of stochastic fluctuations and collective spatial cell behaviour. *PLoS ONE* **5**, e14441.

Tambe, D. T., Hardin, C. C., Angelini, T. E., Rajendran, K., Park, C. Y., Serra-Picamal, X., Zhou, E. H., Zaman, M. H., Butler, J. P., Weitz, D. A. et al. (2011) Collective cell guidance by cooperative intercellular forces. *Nat. Mater.* **10**, 469-475.

Trepat, X., Deng, L., An, S. S., Navajas, D., Tschumperlin, D. J., Gerthoffer, W. T., Butler, J. P. and Fredberg, J. J. (2007). Universal physical responses to stretch in the living cell. *Nature* **447**, 592-595.

Wang, W., Atsushi, T., Mototada, F. and Takehiko, O. (1999). Two-step photodegradation process of poly(ethylene terephthalate). *J. Appl. Polymer Sci.* **74**, 306-310.

Wang, X., Harimoto, K., Liu, J., Guo, J., Hinshaw, S., Chang, Z. and Wang, Z. (2011). Spata4 promotes osteoblast differentiation through Erk-activated Runx2 pathway. *J. Bone Miner. Res.* **26**, 1964-1973.

Webster, T. J., Ergun, C., Doremus, R. H., Siegel, R. W. and Bizios, R. (2000). Enhanced functions of osteoblasts on nanophase ceramics. *Biomaterials* **21**, 1803-1810.

Weitz, D. A. and Janmey, P. A. (2008). The soft framework of the cellular machine. *Proc. Natl. Acad. Sci. USA* **105**, 1105-1106.

Yamamoto, K., Sokabe, T., Watabe, T., Miyazono, K., Yamashita, J. K., Obi, S., Ohura, N., Matsushita, A., Kamiya, A. and Ando, J. (2005). Fluid shear stress induces differentiation of Flk-1-positive embryonic stem cells into vascular endothelial cells in vitro. *Am. J. Physiol.* **288**, H1915-H1924.

Zhang, C., Cho, K., Huang, Y., Lyons, J. P., Zhou, X., Sinha, K., McCrea, P. D. and de Crombrugghe, B. (2008). Inhibition of Wnt signaling by the osteoblast-specific transcription factor Osterix. *Proc. Natl. Acad. Sci. USA* **105**, 6936-6941.

Zouani, O. F., Chollet, C., Guillotin, B. and Durrieu, M. C. (2010). Differentiation of pre-osteoblast cells on poly(ethylene terephthalate) grafted with RGD and/or BMPs mimetic peptides. *Biomaterials* **31**, 8245-8253.